Applied Catalysis A: General 520 (2016) 13–23

Contents lists available at ScienceDirect

Applied Catalysis A: General

journal homepage: www.elsevier.com/locate/apcata

The adsorption of mercury species and catalytic oxidation of Hg^0 on the metal-loaded activated carbon

Lili Fan[a], Lixia Ling[a], Baojun Wang[b,*], Riguang Zhang[b]

[a] College of Chemistry and Chemical Engineering, Taiyuan University of Technology, Taiyuan 030024, Shanxi, People's Republic of China
[b] Key Laboratory of Coal Science and Technology (Taiyuan University of Technology), Ministry of Education and Shanxi Province, Taiyuan 030024, Shanxi, People's Republic of China

ARTICLE INFO

Article history:
Received 19 January 2016
Received in revised form 17 March 2016
Accepted 31 March 2016
Available online 1 April 2016

Keywords:
Mercury species
Metal-loaded AC
Adsorption
Catalytic oxidation

ABSTRACT

The adsorption of mercury species (Hg^0, HgCl and $HgCl_2$) and catalytic oxidation of Hg^0 on the metal-loaded activated carbon (AC) with single Fe, Co, Ni, Cu and Zn atom have been studied using the periodic density functional theory (DFT) method. The results indicate that Hg^0 interacts with metal-loaded AC surfaces via a physical adsorption mechanism, while chemisorptions are likely adsorption mechanisms for HgCl and $HgCl_2$. The existence forms of HgCl and $HgCl_2$ on metal-loaded AC surfaces are dissociated or molecular, which greatly depend on initial interaction modes between mercury species and surfaces. Besides, in the presence of Cl_2, Hg^0 is oxidized to be $HgCl_2$ molecule on the Fe/AC surface, while dissociatively adsorbed $HgCl_2$ is predominant on Ni/AC, Cu/AC and Zn/AC surfaces, but both molecular and dissociated $HgCl_2$ exist on the Co/AC surface. What's more, the kinetic results show that the oxidation energy barrier of Hg^0 on the Fe/AC surface is the lowest, implying that Fe-loaded AC is a favorable heterogeneous catalyst for Hg^0 oxidation from the point of view of efficiency and cost.

1. Introduction

Coal-fired power plants, as a major source of world energy production in the foreseeable future, often cause a series of environmental problems, one of which is the mercury pollution. Mercury is a kind of trace element ranging from 0.01 to 3.3 mg/kg in the coal [1]. During combustion, mercury in the coal will be converted into gaseous elemental mercury at flame temperature and mainly oxidized to be $HgCl_2$ as the flue gas cooling down [2,3]. Once mercury species are released into the atmosphere, adverse health consequences will emerge, including neurological and developmental damages due to their eventual deposition, bioaccumulation and the formation of highly toxic methyl mercury [4]. So controlling the mercury hazards is extremely urgent. Among various mercury forms, oxidized mercury (Hg^{2+}, Hg^+) and particle-bond-mercury (Hg_p) can be removed by wet flue gas desulfurization (WFGD) facilities and air pollution control devices (APCD), respectively. However, the low melting point, high equilibrium vapor pressure and slightly solubility in water of Hg^0 make its capturing to be a huge challenge [2,5]. Thus, it's an urgent concern to develop an economic efficient method for removing mercury.

Up to now, adsorption by sorbents and oxidation of Hg^0 to oxidized mercury are the two typical Hg^0 removal methods [5]. In terms of adsorption, activated carbon (AC) has been studied widely for its large specific surface area and favorable pore size [1,6]. However, the removal efficiency of mercury is very low, especially at high temperature [7,8]. Though chemically impregnated activated carbons with chlorine, sulfur, bromide and iodine have a greater mercury removal capacity than that of the untreated AC, the high cost becomes a great problem [1,9]. In a word, the major obstacles of activated carbon injection technology are its high cost and relatively poor efficiency. Another alternative sorbent is noble metals, which show high Hg^0 removal efficiency with an amalgamation mechanism [6,10,11]. Nevertheless, the application is limited due to the high price [12]. Even worse, the metal monolayer tends to aggregate into larger islands, resulting in the inefficiency of mercury capturing [8]. Thus, neither AC nor noble metals can be widely used to adsorb Hg^0. For the oxidation of Hg^0, it occurs primarily with chlorine radicals (derived from Cl_2 or HCl) through both homogenous and heterogeneous pathways, of which the heterogeneous oxidation is dominant due to the much faster oxidation rate [6,13]. The removal efficiency of Hg^0 greatly depends on the catalyst during the heterogeneous reaction, and the surface composition and structure of a catalyst influence its reaction activity greatly, i.e.

* Corresponding author at: No. 79 West Yingze Street, Taiyuan 030024, People's Republic of China.
E-mail addresses: wangbaojun@tyut.edu.cn, wangbaojunwork@hotmail.com (B. Wang).

http://dx.doi.org/10.1016/j.apcata.2016.03.036
0926-860X/

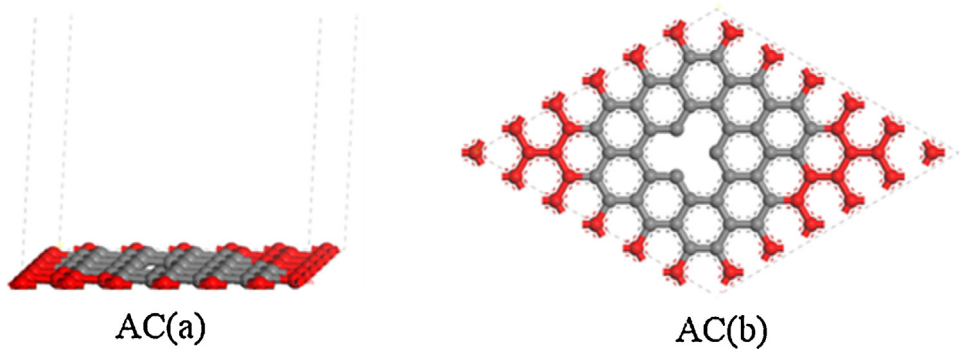

Fig. 1. The optimized slab model of the AC surface. (a) and (b) are the side view and top view of the AC surface, respectively. (The red and dark grey spheres represent the fixed and relaxation carbon atoms, respectively.). (For interpretation of the references to colour in this figure legend, the reader is referred to the web version of this article.)

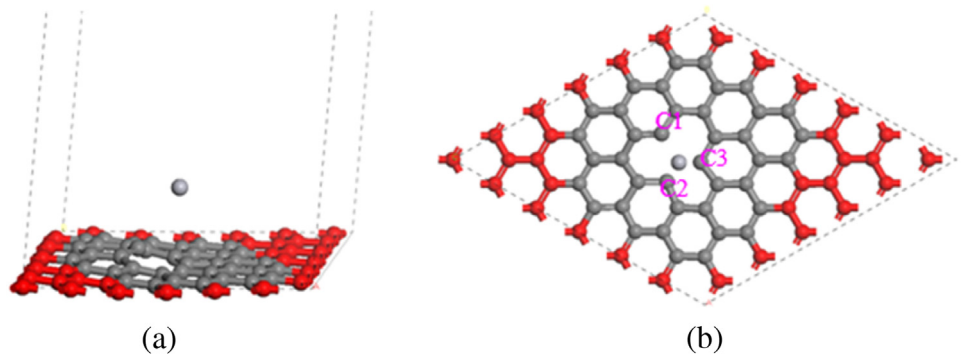

Fig. 2. The optimized adsorption configuration of Hg^0 on the AC surface. (a) and (b) are the side view and top view of Hg^0 adsorption on the AC surface, respectively. (The red, dark grey and light grey spheres represent the fixed C, relaxation C and Hg atoms, respectively.). (For interpretation of the references to colour in this figure legend, the reader is referred to the web version of this article.)

the addition of WO_3 into V_2O_5 can enhance the removal efficiency of Hg^0 [14]. Recently, it's found that there're strong interactions between gas molecules and metal-loaded AC surfaces [15,16–18]. And decorating graphene with transition metal atoms is suggested to be an attractive alternative to improve hydrogen storage capacity [19]. In addition, noble metal modified AC has been widely used to remove Hg^0 with high efficiency [8,10]. It not only improves the capture efficiency of Hg^0, but also reduces the amount of noble metals. In our study, to further reduce the cost of removing Hg^0, non-noble metals should be considered.

At present, experimental studies of Hg^0 adsorption on Cu and Ni surfaces have been carried out, showing that there's a strong chemisorption on the Ni(001) surface, and copper has a high affinity to Hg^0 [20,21]. Additionally, Fe(100), Ni(100), Cu(100) and Zn surface also show strong interactions with Hg^0 [21,22]. Adsorption energies of Hg^0 on the Cu(111) are 62.4 and 63.1 kJ/mol on the fcc site and hcp site, respectively [23]. And the Cu(001) surface has a stronger interaction with Hg^0 than that of Cu(111) surface [6]. On the Zn surface, Hg^0 can react with the Predeposited chlorine and form $HgCl_2$ [21]. Besides, it has also found that Fe, Co, Ni and Cu can be stable as isolated atoms on the graphitic carbon surface, resulting in an increase of its catalytic activity [15,24,25]. For example, Fe/G (Fe/graphene) is more sensitive to the adsorption of H_2S and CO than that of the pristine graphene, and compared to Ni-G and Cu-G, Fe/G and Co/G show stronger interactions with CO molecule [12,15,24]. Meanwhile, Zheng *et al.* [25] also found that the dissociation barriers of O_2 on Co/G and Ni/G are lower than that on pristine-G and N-G, showing that the doped-G with Co and Ni are promising oxygen reduction reaction catalysts. Synchronously, the Ni-doped graphene is more sensitive to the tyrosine nitration than the intrinsic graphene and might be a good choice for the protein tyrosine nitration (PTN) detection [26]. However, the removal efficiency and mechanism of Hg^0 by non-noble metal loaded AC are not clear.

In this work, to highlight the effect of loaded non-noble metal atoms on Hg^0 removal, adjacent main group elements Fe, Co, Ni, Cu and Zn are chosen. Firstly, Hg^0 adsorption on the pure AC surface is studied. Then, the adsorption of mercury species (Hg^0, HgCl and $HgCl_2$) and oxidation of Hg^0 by Cl_2 under the catalysis of metal-loaded AC surfaces are investigated. Finally, the catalytic oxidation processes of Hg^0 are discussed, along with which is the selection of the optimal catalyst.

2. Calculation method and the model

2.1. Computation method

The DMol^3 program package in Materials Studio 5.5 was selected for the following periodic density functional (DFT) calculation [12,27]. GGA with Perdue-Wang exchange-correlation functional (PW91) was designated to calculate the exchange and correlation energies [28]. For relativistic effects, the inner electrons of Fe, Co, Ni, Cu, Zn and Hg atoms were kept frozen and replaced by an effective core potentials (ECP), while an all-electron basis set was applied to treat with other atoms [7]. During calculations, no symmetry and spin polarization were considered for the existence of the carbon vacancies, which induce magnetism by breaking the symmetry of the nonmagnetic perfect graphite surface [29]. For valence electron functions, the doubled-numerical quality basis set with polarization functions (DNP) was employed [15]. Based on test results, the real space cutoff radius was set to be 4.6 Å. By calculating one Cu atom adsorption on the AC surface in different

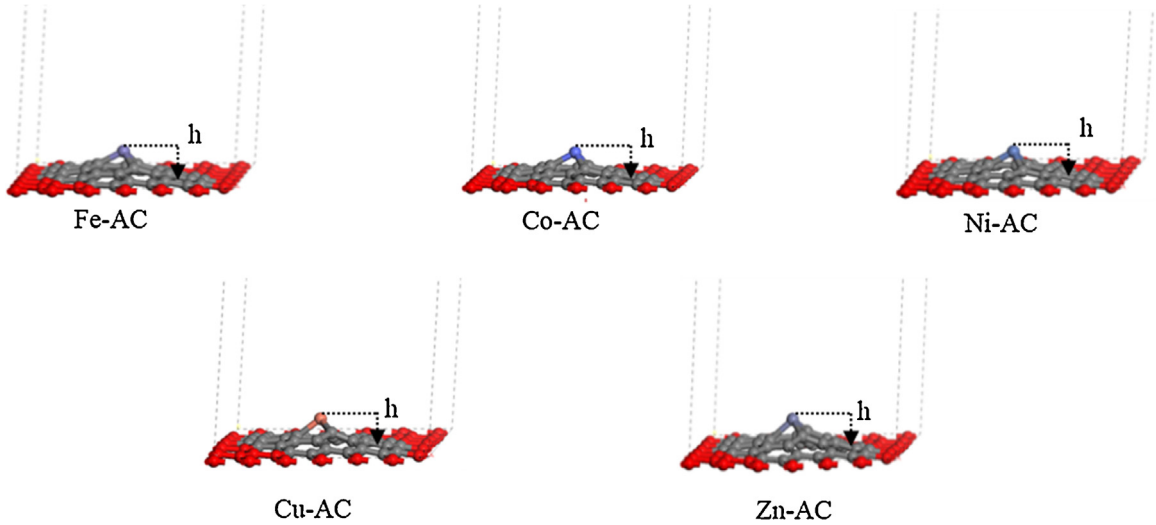

Fig. 3. The optimized adsorption configurations of Fe, Co, Ni, Cu and Zn on the AC surface. (The protuberant, red and dark grey spheres represent the loaded metal, fixed C and relaxation C atoms, respectively.). (For interpretation of the references to colour in this figure legend, the reader is referred to the web version of this article.)

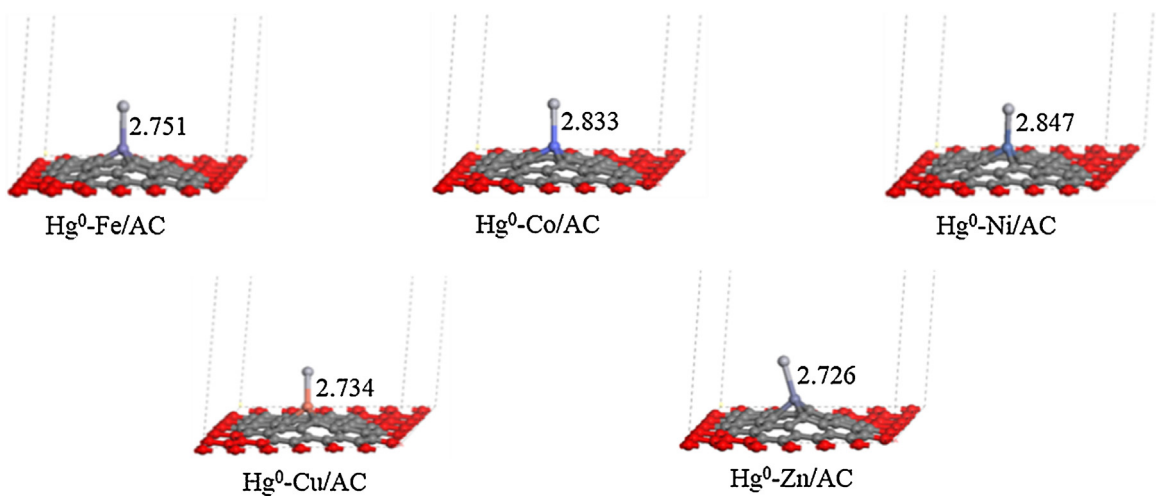

Fig. 4. The optimized adsorption configurations of Hg^0 on M/AC (M = Fe, Co, Ni, Cu and Zn) surfaces. (The red, dark grey, light grey and protuberant spheres represent the fixed C, relaxation C, Hg and the loaded metal atoms, respectively.). (For interpretation of the references to colour in this figure legend, the reader is referred to the web version of this article.)

k-point ($3 \times 3 \times 1$, $5 \times 5 \times 1$ and $7 \times 7 \times 1$), total energy convergence (2×10^{-5}, 2×10^{-6} and 2×10^{-7} Ha) and force displacement convergence (4×10^{-3}, 4×10^{-4} and 4×10^{-5} Ha/Å), it's found that there's almost no energy difference. Hence, like some other studies, we choose $3 \times 3 \times 1$ *k*-point for all the calculations [30,31]. The total energy and force displacement converged to 2×10^{-5} Ha and 4×10^{-3} Ha/Å, respectively.

For the purpose of determining the activation barriers of Hg^0 oxidation, we choose the complete LST/QST method to search the transition states (TS) of reactions. The LST (Linear Synchronous Transit) method performs a single interpolation to a maximum energy from reactants to products, and the QST (Quadratic Synchronous Transit) method alternates searches for an energy maximum with constrained minimization, which refines the transition states to a high degree [32]. In the meantime, transition state conformations and frequency analyses were performed, which not only can demonstrate that each transition state leads to the desired reactants and products but also can ensure the rationality of reactants, transition states and products.

The adsorption energies (E_{ads}) of relative species and activation energies of elementary steps are calculated according to the following equations:

$$E_{ads} = E_{(support)} + E_{(adsorbate)} - E_{(adsorbate/support)} \quad (1)$$

$$E_a = E_{TS} - E_R \quad (2)$$

where $E_{(adsorbate)}$ is the total energy of the free adsorbate in the gas phase, $E_{(support)}$ is the total energy of the support, $E_{(adsorbate/support)}$ is the total energy of the support and adsorbate in its equilibrium geometry, E_a is the activation energy of the elementary step, E_{TS} is the total energy of the transition state and E_R is the total energy of the reactant. Based on above definitions, it can be concluded that a positive value of adsorption energy corresponds to a stable adsorption and a more positive value implies a stronger interaction between adsorbed species and surface atoms. Meanwhile, a smaller value of the activation energy means a more favorable kinetic process.

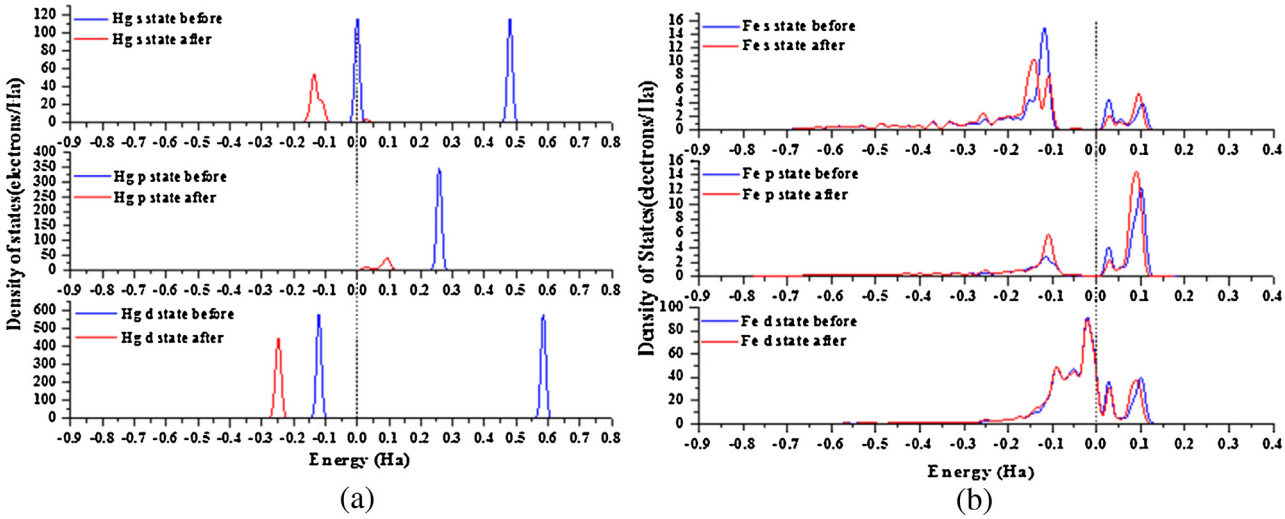

Fig. 5. PDOS for the surface system before and after Hg^0 adsorption on the Fe/AC surface. (a) and (b) are the PDOS of the *s*, *p* and *d* orbitals for Hg atom and Fe atom, respectively. (The blue and red lines represent the situations adsorbed before and after, respectively.). (For interpretation of the references to colour in this figure legend, the reader is referred to the web version of this article.)

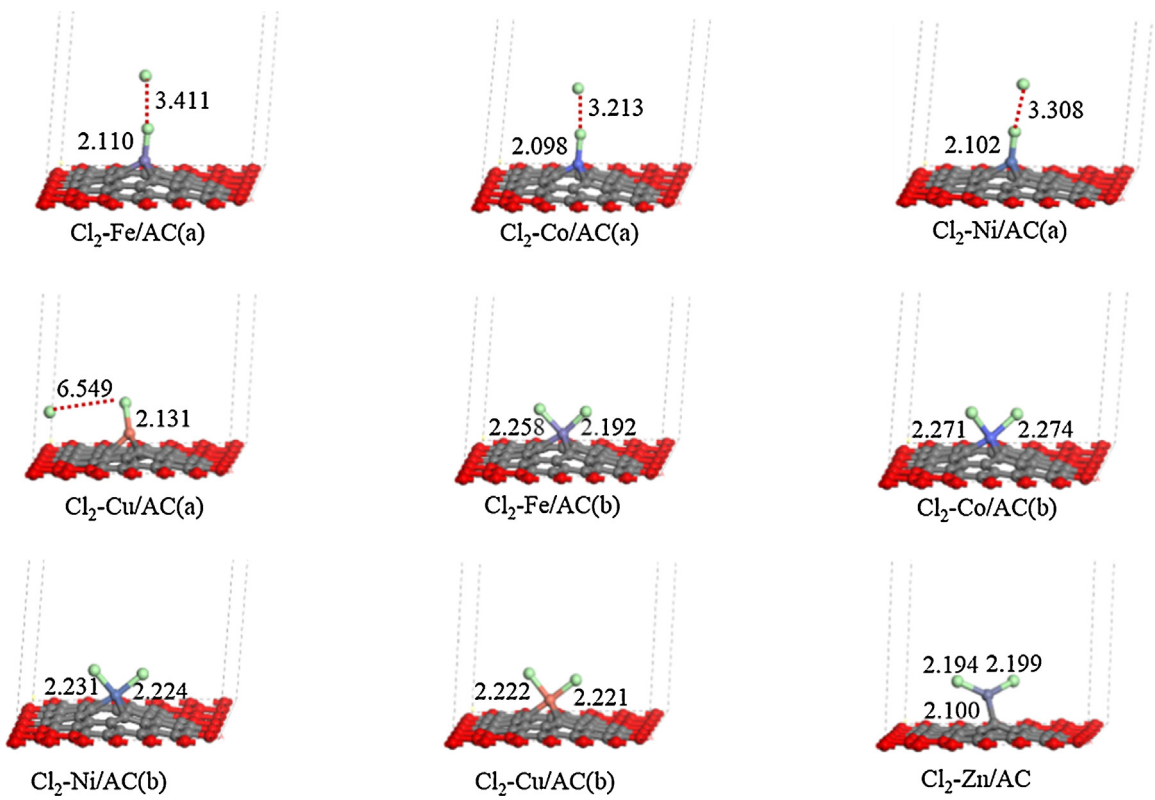

Fig. 6. The optimized geometries of Cl_2 adsorption on M/AC (M = Fe, Co, Ni, Cu and Zn) surfaces. In figures (a) and (b), Cl_2 is placed vertically and parallel to the substrates, respectively. (The red, dark grey, light grey and green spheres represent the fixed C, relaxation C, Hg and Cl atoms, respectively.). (For interpretation of the references to colour in this figure legend, the reader is referred to the web version of this article.)

2.2. Surface model

The structure of activated carbon is very complex, but the basic structural unit is the graphite platelet [33]. Thus, a graphite platelet is built to model the AC surface. However, the actual AC is not perfect, which contains disordered defective crystallites of graphite [33]. It has been reported that vacancies on the carbon material affect its reactivity greatly [34]. And among Stone-Wales (SW) defect, single vacancy (SV) defect and double vacancy (DV) defect of graphite platelet, only the single vacancy (SV) defect is highly active and studied widely [35–38]. Up to now, different periodic or cluster models of graphite have been built to describe the adsorption and reaction on AC surface [33,39–41]. In this study, a single-layer graphite with single defect is built to model the AC surface by cleaving the optimized graphite structure with lattice parameters of a = b = 2.468 Å. Moreover, considering the interactions between periodic vacancy defects, it is necessary to fix the surface carbon atoms at the largest distance from the vacancy site

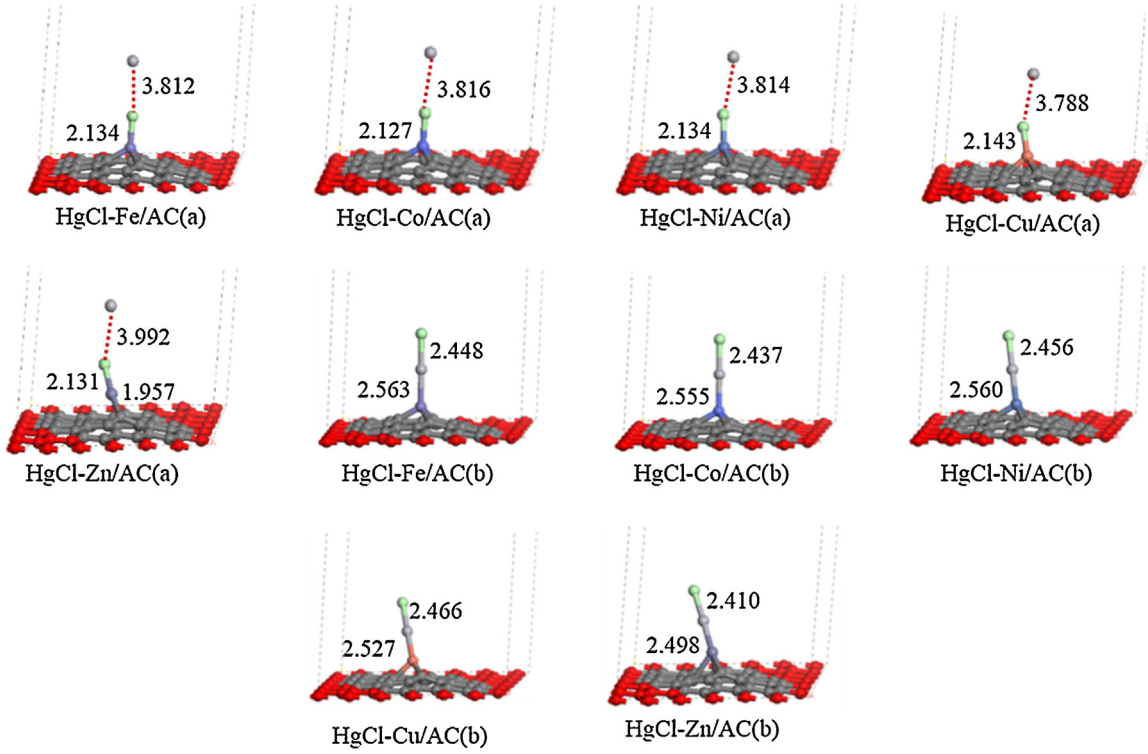

Fig. 7. The stable adsorption configurations of HgCl on M/AC (M = Fe, Co, Ni, Cu and Zn) surfaces. (The red, dark grey, light grey and green spheres represent the fixed C, relaxation C, Hg and Cl atoms, respectively.). (For interpretation of the references to colour in this figure legend, the reader is referred to the web version of this article.)

until there appears a distinct energy difference compared to the fully relaxed graphene model. [31,37]. In this research, the fixed atoms are marked in red, as shown in Fig. 1.

Hg^0 adsorption behaviors on AC surfaces with p(5 × 5), p(6 × 6) and p(7 × 7) slabs are studied, and adsorption energies are 9.2, 27.2 and 31.1 kJ/mol, respectively. It can be seen that when the surface size enlarges to 7 × 7 from 6 × 6, the increment of adsorption energy is much smaller than that between 5 × 5 and 6 × 6 surfaces. Thus, a 6 × 6 supercell is reasonable, which has also been used to study adsorptions of gas molecules (O_2, CO, NO_2, NH_3 and CO_2) on the AC surface [15,37,38,42]. To avoid the interactions between periodic images, a 15 Å vacuum region was added to the slab. Fig. 1 shows the optimized AC model, in which AC(a) and AC(b) are the side view and top view, respectively.

3. Results and discussion

3.1. Assessment of the method and surface model

Depending on the selected calculation method and parameters, the optimized graphite's lattice constant is determined as 2.468 Å, which is in good agreement with the experimental value of 2.485 Å and other calculated values of 2.467 and 2.468 Å [43,44]. What's more, the calculated adsorption energy of H_2S on the Fe-doped graphite layer is 105.6 kJ/mol, also close to the literature value of 98.6 kJ/mol [12]. Thus, the calculation model, parameters and method adopted in our work are reliable.

3.2. Adsorption of Hg^0 on the AC surface

Initially, Hg^0 is placed on the SV site, the only active site of AC. The optimized adsorption configuration of Hg^0 on the AC surface is presented in Fig. 2, in which (a) is the side view and (b) is the top view. The adsorption energies, C—Hg bond lengths and charge transfers of Hg^0 are given in Table 1. It can be learnt that

Table 1
The adsorption energies (E_{ads}, kJ/mol), Mulliken charge transfer (Q, e) and distances (R, Å) between Hg^0 and its adjacent carbon atoms involved in Hg^0 adsorption on the AC surface.

Species	R_{Hg^0-Cx}	Q_{Hg}	E_{ads}
Hg^0	(C1) 3.476 (C2) 3.988 (C3) 4.019	0.001	27.4

there's a weak interaction between Hg^0 and the AC surface with an adsorption energy of 27.4 kJ/mol, and the distances between Hg^0 and C1, C2 and C3 are 3.467, 3.988, and 4.019 Å, respectively. In addition, Mulliken population analysis indicates that only 0.001e charge transfers from Hg^0 to the AC surface. Therefore, it can be concluded that Hg^0 is physically bound to the AC surface, which is in agreement with the experimental and theoretical investigations [2,45].

3.3. Adsorptions of mercury species and Cl_2 on the M/AC (M = Fe, Co, Ni, Cu and Zn)

Before studying the adsorption behaviors of mercury species on Fe/AC, Co/AC, Ni/AC, Cu/AC and Zn/AC, it's vital to ensure their stability. Fig. 3 shows the corresponding stable configurations, from which we can see that the SV site on the AC surface acts as a trapping site for the single-metal-atom, consistent with the previous work [15]. Besides, as other investigations, the much larger radius of metal atoms than that of carbon leads to Fe, Co, Ni, Cu and Zn extruding outwards from the AC surface [38,46], and the height h are displayed in Table 2. What's more, the adsorption energies of Co, Fe, Ni, Cu and Zn on the AC surface are 761.8, 695.1, 647.4, 347.7 and 116.5 kJ/mol, respectively. They are in agreement with literature calculation values of 743.0, 704.4, 656.1, 328.1 and 115.8 kJ/mol, further proving the rationality of our calculation parameters and method [46]. It can be seen that the adsorption energy of Zn atom

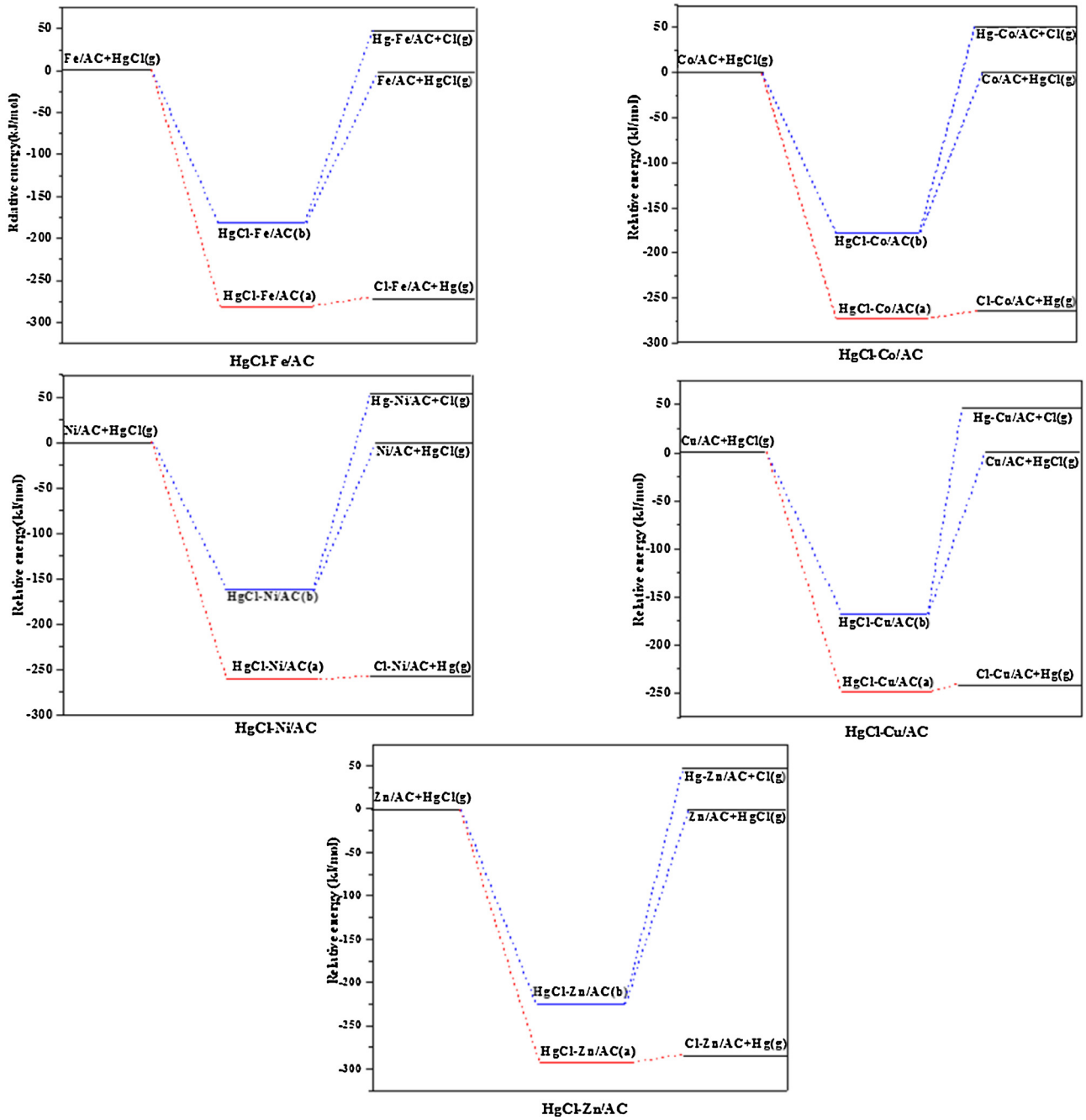

Fig. 8. Potential energy diagrams for HgCl adsorption on M/AC (M = Fe, Co, Ni, Cu and Zn).

Table 2
The adsorption energies (E_{ads}, kJ/mol) and protrusion height (h, Å) involved in the adsorption of Fe, Co, Ni, Cu and Zn on the AC surface.

Species	h	E_{ads}	
		Cal.	*Ref.*
Fe	1.625	695.1	704.4
Co	1.565	761.8	743.0
Ni	1.513	647.4	656.1
Cu	1.639	347.7	328.1
Zn	1.843	116.5	115.8

on the AC is the smallest, but it is still a strong chemical adsorption. Therefore, Fe, Co, Ni, Cu and Zn atoms can be loaded on the AC surface stably, in agreement with previous studies [15,24,25].

3.3.1. Hg^0 adsorption

For Hg^0 adsorption, both loaded metals and the carbons neighboring the metal are considered as adsorption sites. However, the latter are not stable adsorption sites for Hg^0 adsorption. Instead, when Hg^0 is placed on the carbon neighboring the metal, it migrates to the loaded metal atom. The stable adsorption configurations of Hg^0 on metal-loaded AC surfaces are shown in Fig. 4, and Table 3 shows the corresponding adsorption energies, bond lengths and Mulliken charge transfer. It can be seen that adsorption energies of Hg^0 on M/AC (M = Fe, Zn, Cu, Co, and Ni) surfaces show a continued decreasing trend, but the variation of Hg-M distances are not monotonous. When compared to the adsorption energy of Hg^0 on the untreated AC surface with 27.4 kJ/mol, a conclusion can be drawn that loading transition metal atoms Fe, Co, Ni, Cu and Zn on

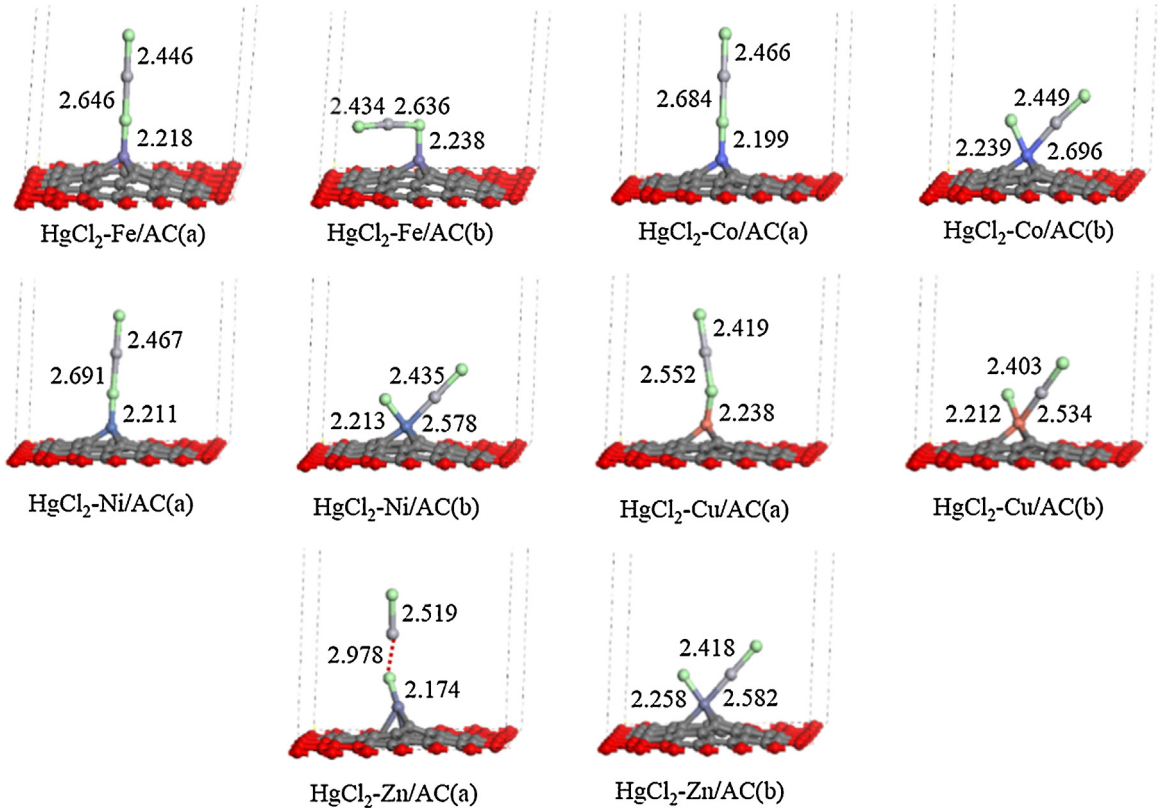

Fig. 9. The optimized adsorption geometries of $HgCl_2$ on M/AC (M = Fe, Co, Ni, Cu and Zn) surfaces. In figures (a) and (b), $HgCl_2$ is placed vertically and parallel to the substrates, respectively. (The red, dark grey, light grey and green spheres represent the fixed C, relaxation C, Hg and Cl atoms, respectively.). (For interpretation of the references to colour in this figure legend, the reader is referred to the web version of this article.)

Table 3
The adsorption energies (E_{ads}, kJ/mol), bond lengths (Å) and Mulliken charge transfer (Q, e) involved in the adsorption of mercury species Hg^0, HgCl and $HgCl_2$ on M/AC (M = Fe, Co, Ni, Cu and Zn) surfaces.

Surface	Species	R_{Hg^0-M}	E_{ads}	Q_{Hg}	Species	E_{ads}	Species	E_{ads}
Fe/AC	Hg^0	2.751	40.3	0.112	HgCl(a)	280.9	$HgCl_2$(a)	84.4
					HgCl(b)	180.3	$HgCl_2$(b)	100.4
Co/AC	Hg^0	2.833	31.3	0.067	HgCl(a)	272.4	$HgCl_2$(a)	79.7
					HgCl(b)	177.6	$HgCl_2$(b)	81.5
Ni/AC	Hg^0	2.847	30.0	0.053	HgCl(a)	260.7	$HgCl_2$(a)	67.7
					HgCl(b)	162.6	$HgCl_2$(b)	122.2
Cu/AC	Hg^0	2.734	35.9	0.091	HgCl(a)	249.5	$HgCl_2$(a)	60.7
					HgCl(b)	167.7	$HgCl_2$(b)	124.2
Zn/AC	Hg^0	2.726	36.4	0.109	HgCl(a)	294.0	$HgCl_2$(a)	83.2
					HgCl(b)	225.1	$HgCl_2$(b)	79.8

Notes: HgCl-M/AC(a) and HgCl-M/AC(b) are the Cl-down and Hg-down cases, respectively. $HgCl_2$-M/AC(a) and $HgCl_2$-M/AC(b) represent the initial parallel and vertical placement modes, respectively.

the AC surface is favorable for the adsorption of Hg^0, but still a weak physical interaction.

To interpret interactions between Hg^0 and metal-loaded AC surfaces, Mulliken population analysis has been carried out. The result shows that after interacting with Fe/AC, Zn/AC, Cu/AC, Co/AC and Ni/AC surfaces, Hg atoms are positively charged with 0.112, 0.109, 0.091, 0.067 and 0.053 e, respectively. It can be seen that the interaction between Hg^0 and Fe/AC is the strongest, Zn/AC is secondary, Co/AC and Ni/AC are the weakest. Besides, Bader charge analysis is also performed by VASP (Vienna Ab-initio Simulation) software, showing a consistent result, with electron transfer of 0.0610, 0.0574, 0.0366, 0.0021 and 0.0027 e on Fe/AC, Zn/AC, Cu/AC, Co/AC and Ni/AC surfaces, respectively.

In addition, to further elucidate the adsorption mechanism of Hg^0 on the metal-loaded AC surface, the density of states (DOS) for surface atoms has also been analyzed. The DOS of a system possesses a function of depicting the number of states per interval of energy at each energy level that are available to be occupied by electrons [47]. Since the division of atomic orbital is based on energy differences, the partial density of states (PDOS) of each atom can reflect the distribution of electrons in each orbit. It not only can analyze the bonding of atoms but also can show the occupancy of electrons on each orbital. For example, the shift down of atom states means a bonding of atoms and greater hybridization of states leads to a stronger bond. Then their interactions and nature of bonding can be well understood and revealed by analyzing the PDOS of bonding atoms.

In our study, the partial density of states (PDOS) of the Hg atom and the loaded Fe atom are analyzed, which are shown in Fig. 5. After the isolated Hg atom interacting with the Fe/AC surface, all the states of Hg atom shift down. However, only p state slightly broadened and the sharp peaks of s and d states are not changed, implying a weak interaction between Hg^0 and the Fe/AC surface. Similarly, after interacting with $MnO_2(110)$ and $ZnO(10\bar{1}0)$ surfaces, the states of Hg atom shift down and the sharp peak of d state is not changed. Also, variations exist in the p state of Hg atom. On the $ZnO(10\bar{1}0)$ surface, the p states of Hg atom broadens slightly, which is similar to that on the Fe/AC surface [32]. But differently, the p state of Hg atom disappears after interacting with the $MnO_2(110)$ surface [47]. In addition, there are almost no change for s, p and d states of loaded Fe before and after interacting with Hg.

Meanwhile, there are two very narrow hybridized regions between the p state of Fe and s state of Hg at −0.16–−0.09 Ha, as

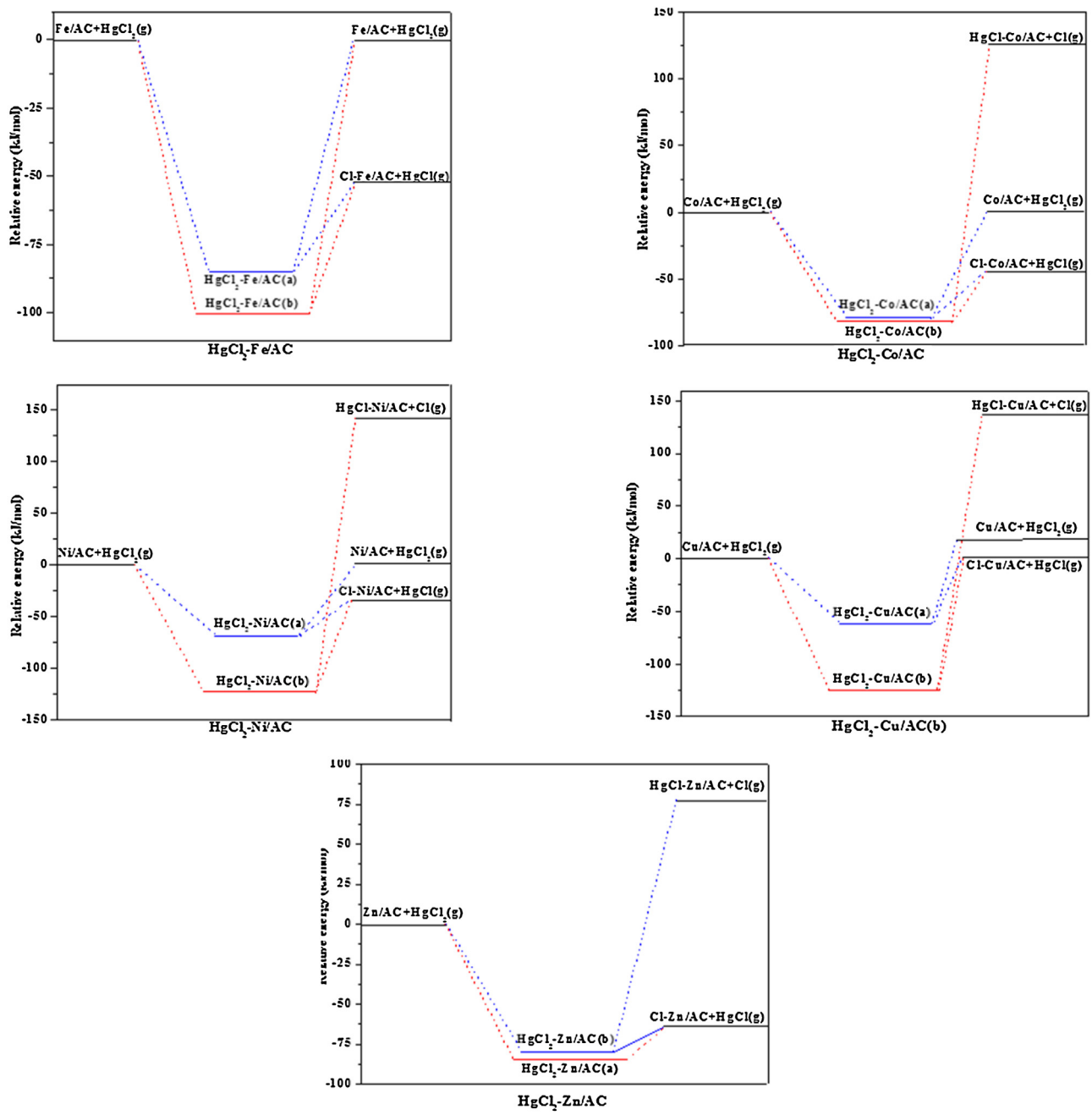

Fig. 10. Potential energy diagrams for $HgCl_2$ adsorption on M/AC (M = Fe, Co, Ni, Cu and Zn).

well as between the *p* state of Fe and *p* state of Hg at 0.05–0.12 Ha, respectively. Based on the above analysis, it can be concluded that the interaction between Hg^0 and the Fe/AC surface is weak.

All the illustrations above indicate that Hg^0 only has a physical interaction with the Fe/AC surface and it can be inferred that the same adsorption mechanisms are for Hg^0 adsorption on Co/AC, Ni/AC, Cu/AC and Zn/AC surfaces. Similarly, the adsorption behaviors of Hg^0 on the α-Fe_2O_3(001), ZnO(10$\bar{1}$0) and CaO(001) also indicate physisorption mechanisms, with adsorption energies of 37.7, 27.0 and 27.3 kJ/mol, respectively [48,32,49]. additionally, it is also a physical interaction with an adsorption energy of 40.6 kJ/mol when Hg^0 adsorbs on the perfect noble Au(111) surface [50].

3.3.2. Cl_2 adsorption

For the oxidation of Hg^0 by Cl_2, the activated species is Cl radical, which is derived from the dissociation of Cl_2. Thus, investigating the activation process of Cl_2 to be Cl radical on M/AC (M = Fe, Co, Ni, Cu, and Zn) surfaces is necessary. Initially, Cl_2 is placed on each surface in vertical and parallel modes, respectively. And activated states of Cl_2 on metal-loaded AC surfaces are shown in Fig. 6. Under the catalysis of Fe/AC, Co/AC, Ni/AC and Cu/AC, two kinds activated states of Cl_2 are obtained. In terms of Cl_2-Fe/AC (a), Cl_2-Co/AC (a), Cl_2-Ni/AC (a) and Cl_2-Cu/AC (a), only a Cl radical adsorbs on surfaces, leaving the other Cl radical rejected to distances of 3.411, 3.213, 3.308 and 6.549 Å, respectively. Cl_2-Fe/AC (b), Cl_2-Co/AC (b), Cl_2-Ni/AC (b) and Cl_2-Cu/AC (b) represent the other activation type, of which two Cl radicals adsorb on surfaces jointly. Differently, only one kind activation product is achieved on the Zn/AC surface and the configuration is shown in the Cl_2-Zn/AC. Besides, adsorption energies involved in activated processes of Cl_2 are displayed in Table 4, showing strong interactions between Cl_2 and metal-loaded AC surfaces. Importantly, it can be discovered that during the acti-

Table 4
The adsorption energies (E_{ads}, kJ/mol) and bond lengths (Å) involved in the activations of Cl_2 on M/AC (M = Fe, Co, Ni, Cu and Zn) surfaces. In Cl_2-M/AC(a) and Cl_2-M/AC(b), Cl_2 is placed vertically and parallel to the substrates, respectively.

Configuration	R_{Cl-M}	R_{Cl-Cl}	E_{ads}	Configuration	R_{Cl-M}		E_{ads}
Cl_2-Fe/AC(a)	2.110	3.411	167.8	Cl_2-Fe/AC(b)	2.258	2.192	238.0
Cl_2—Co/AC(a)	2.098	3.213	171.7	Cl_2—Co/AC(b)	2.271	2.274	245.6
Cl_2—Ni/AC(a)	2.102	3.308	164.5	Cl_2—Ni/AC(b)	2.231	2.224	299.8
Cl_2—Cu/AC(a)	2.131	6.549	172.2	Cl_2—Cu/AC(b)	2.222	2.221	280.8
				Cl_2-Zn/AC	2.194	2.199	345.0

vation of Cl_2 molecule to be Cl radical, each metal-loaded AC serves as an excellent medium, resembling with the role of Au catalyst in the Hg^0 oxidation by Cl_2 [51].

3.3.3. HgCl adsorption

During the catalytic oxidation process of mercury, HgCl is an important intermediate, which leads to the investigation of HgCl adsorption on metal-loaded AC surfaces an indispensable case [32,52]. To comprehensively describe adsorption processes of HgCl, both parallel and vertical adsorption cases are taken into consideration and their stable adsorption configurations are shown in Fig. 7. For Cl-down cases, as shown in Fig. 7a, strong interactions between M/AC (M = Fe, Co, Ni, Cu and Zn) surfaces and Cl lead to stretches of Hg—Cl bonds, with distances of 3.812, 3.816, 3.814, 3.788 and 3.992 Å, respectively. Fig. 7b shows Hg-down cases, it can be seen that HgCl molecularly adsorbs on M/AC (M = Fe, Co, Ni, Cu and Zn) surfaces. Besides, adsorption energies involved in HgCl adsorption are listed in Table 3.

The potential energy diagrams for different pathways of HgCl adsorption on Fe/AC, Co/AC, Ni/AC, Cu/AC and Zn/AC surfaces are shown in Fig. 8. It can be seen that dissociated adsorption configurations are more likely to form for their more exothermic property. Also, only 6.3, 6.4, 4.7, 7.3 and 8.2 kJ/mol energies are needed for Cl adsorption on the surfaces and Hg desorption, respectively. It's suggested that in Cl-down cases HgCl-Fe/AC (a), HgCl-Co/AC (a), HgCl-Ni/AC (a), HgCl-Cu/AC (a) and HgCl-Zn/AC (a), HgCl inclines to the dissociated adsorption. However, for Hg-down modes, HgCl prefers the molecular adsorption, shown in HgCl-Fe/AC (b), HgCl-Co/AC (b), HgCl-Ni/AC (b), HgCl-Cu/AC (b) and HgCl-Zn/AC (b). In addition, the dissociation of HgCl with Hg adsorption on surfaces and Cl desorption is highly endothermic by 222.6, 228.9, 215.2, 214.4 and 271.4 kJ/mol, respectively. And for the desorption of HgCl, energies of 180.3, 177.6, 162.6, 167.7 and 225.1 kJ/mol are needed to supply, respectively. Therefore, HgCl molecule can adsorb on Fe/AC, Co/AC, Ni/AC, Cu/AC and Zn/AC surfaces firmly in Hg-down mode.

All analyses above indicate that HgCl adsorbs on metal-loaded AC surfaces in two modes. For the Cl-down case, HgCl prefers to dissociate with Cl binding on AC surfaces and Hg desorbing. For the Hg-down case, HgCl goes through the molecular adsorption. But structures shown as HgCl-M/AC (a) in Fig.7 are more likely to form, consistent with HgCl adsorption on ZnO(10$\bar{1}$0), α-Fe2O3(001) and CaO(100) surfaces. [32,48,53].

3.3.2. $HgCl_2$ adsorption

The development of mercury control technologies has made progress, but there still no single best control technology can be broadly applied currently. Based on the fact that oxidized mercury is easily removed, transforming Hg^0 into the oxidized state is regarded as a promising method for mercury removal [54,55]. Then, the following study mainly focuses on the adsorption of $HgCl_2$, the main oxidation state of mercury in the flue gas [6].

$HgCl_2$ is initially placed on Fe/AC, Co/AC, Ni/AC, Cu/AC and Zn/AC surfaces in vertical and parallel orientations. The optimized adsorption configurations and energies involved in each adsorption process are shown in Fig. 9 and Table 3, respectively. For $HgCl_2$ adsorption on the Fe/AC surface, two molecular adsorption configurations $HgCl_2$-Fe/AC (a) and $HgCl_2$-Fe/AC (b) are obtained, representing the vertical and parallel molecular adsorption structures, respectively. Simultaneously, for $HgCl_2$-Fe/AC (b), the adsorption energy is 100.4 kJ/mol, 16.0 kJ/mol higher than that of $HgCl_2$-Fe/AC (a), implying a parallel molecular adsorption inclination. Similarly, the same cases happen on ZnO(10$\bar{1}$0), CaO(100) and V_2O_5(001) surfaces, with adsorption energies of 116.8, 89.9 and 76.3 kJ/mol, respectively [32,52,53].

Differently, $HgCl_2$ adsorbs on Co/AC, Ni/AC and Cu/AC surfaces both molecularly and dissociatively. For the perpendicular cases, $HgCl_2$ adsorbs on surfaces in molecular mode, shown in $HgCl_2$-Co/AC (a), $HgCl_2$-Ni/AC (a) and $HgCl_2$-Cu/AC (a), respectively. $HgCl_2$-Co/AC (b), $HgCl_2$-Ni/AC (b) and $HgCl_2$-Cu/AC (b) are the parallel cases, with Cl atom and HgCl molecular adsorbing on surfaces jointly. Besides, the angles between Hg and Cl decrease to 73.4°, 81.9° and 80.3°, respectively. Comparing adsorption energies of $HgCl_2$ on metal-loaded AC surfaces, it can be seen that both molecular and dissociated configurations of $HgCl_2$ are existent on the Co/AC surface, but $HgCl_2$-Ni/AC (b) and $HgCl_2$-Cu/AC (b) are preferred on Ni/AC and Cu/AC surfaces, resembling with the cases on the α-Fe_2O_3(001) surface that HgCl molecular and Cl atom adsorb on the surface together [48]. Particularly, $HgCl_2$ adsorbs on the Zn/AC surface via two kinds dissociated modes, which are shown in $HgCl_2$-Zn/AC (a) and $HgCl_2$-Zn/AC (b), with adsorption energies of 83.2 kJ/mol and 79.8 kJ/mol, respectively.

In addition, a close examination of the energy diagrams for different pathways of $HgCl_2$ adsorption on M/AC (M = Fe, Co, Ni, Cu and Zn) surfaces are shown in Fig. 10. For the adsorption of $HgCl_2$ on Fe/AC, Ni/AC and Cu/AC surfaces, $HgCl_2$-Fe/AC (b), $HgCl_2$-Ni/AC (b) and $HgCl_2$-Cu/AC (b) are more likely to form since the pathways are more exothermic. Besides, either desorption or dissociation of $HgCl_2$ needs large energies to supply, implying a stable molecular adsorption of $HgCl_2$ on the Fe/AC surface, while dissociated $HgCl_2$ is preferred on Ni/AC and Cu/AC (b) surfaces with Cl and HgCl molecular adsorbing on surfaces jointly. Differently, both $HgCl_2$-Co(Zn)/AC (a) and $HgCl_2$-Co(Zn)/AC (b) are existent for their similar exothermic properties. And only a little energy is required for the strong binding of Cl on the Co(Zn)/AC surfaces and desorption of HgCl into the gas phase.

In conclusion, the main existence forms of $HgCl_2$ on metal-loaded AC surfaces are various. On the Fe/AC surface, $HgCl_2$ inclines to the molecular adsorption $HgCl_2$-Fe/AC (b), while dissociated adsorptions are primary to Ni/AC[$HgCl_2$-Ni/AC (b)], Cu/AC[$HgCl_2$-Cu/AC (b)] and Zn/AC[$HgCl_2$-Zn/AC (a) and $HgCl_2$-Zn/AC (b)] surfaces. But both molecular and dissociated adsorption cases exist on the Co/AC surface. In addition, it can be seen that only a little energy supply can lead to the occurrence of Cl-Co/AC + HgCl (g) and Cl-Zn/AC + HgCl (g).

3.3.3. The adsorption properties of mercury species

Based on the calculation results, it is known that Hg^0 can not be removed by the metal-loaded AC for its physical adsorption. Though HgCl inclines to a chemisorption, it's not feasible to remove Hg^0 in the form of HgCl, which mainly exists in the dissociated scenario with Cl adsorbed on metal-loaded AC surfaces and Hg desorbed. $HgCl_2$ adsorbs on metal-loaded AC surfaces molecularly or dissociatively, implying that oxidizing Hg^0 to $HgCl_2$ is a practicable Hg^0 removal method and discussed in the following study.

3.4. The catalytic oxidation of Hg^0 by Cl_2

According to studies above, it is known that Cl atoms have much stronger interactions with metal-loaded AC surfaces than that of Hg^0, which has also been verified by Mulliken population analysis further. The result shows that electron transfer between Cl_2 and

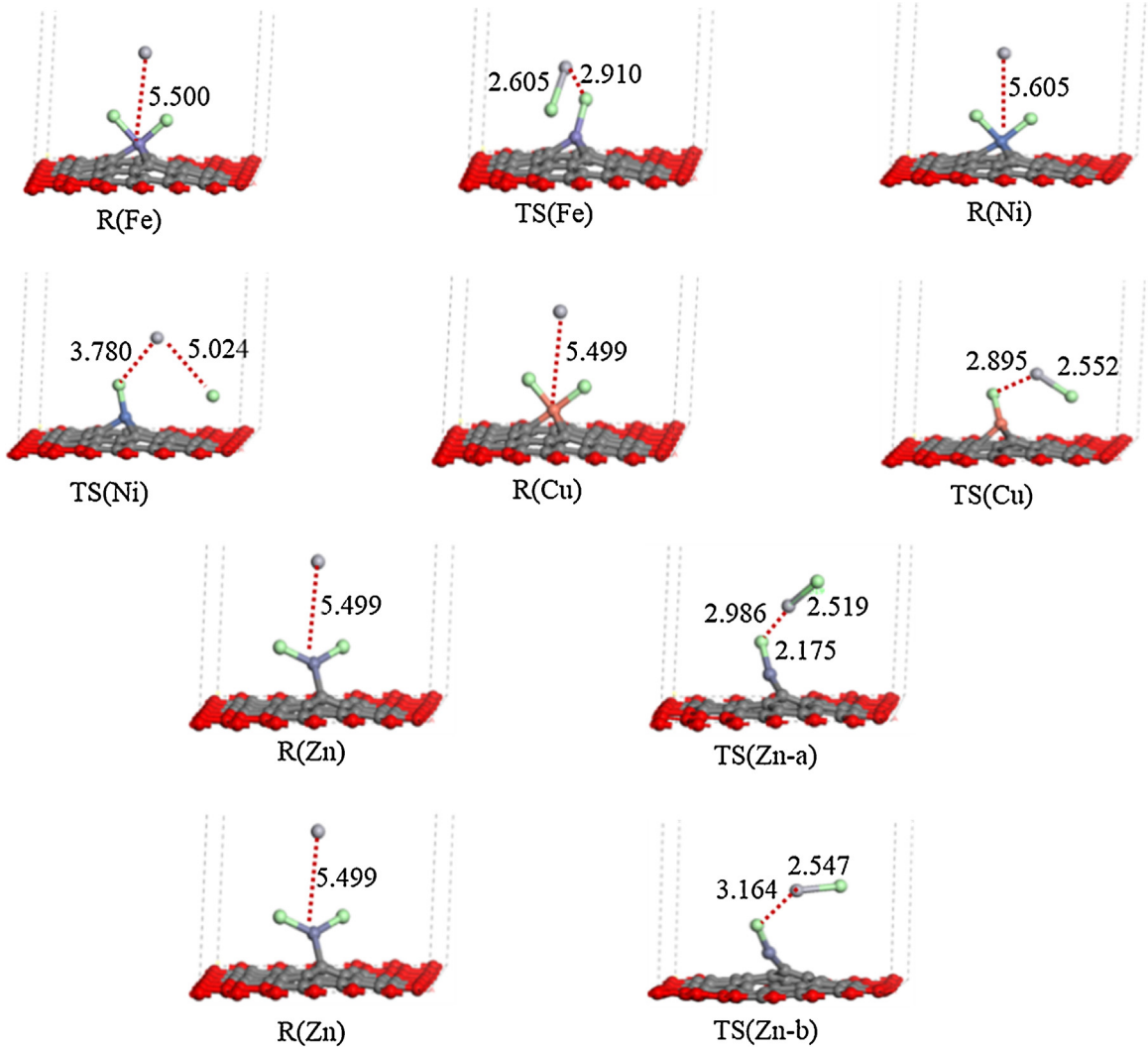

Fig. 11. The configurations of reactants, transition states and products involved in the oxidation processes of Hg^0 on 2Cl-M/AC (M = Fe, Ni, Cu and Zn) surfaces. (The red, dark grey, light grey and green spheres represent the fixed C, relaxation C, Hg and Cl atoms, respectively.). (For interpretation of the references to colour in this figure legend, the reader is referred to the web version of this article.)

M/AC (M = Fe, Co, Ni, Cu, and Zn) surfaces are 0.554, 0.555, 0.639, 0.468, 0.697 *e*, respectively, much more than that between Hg^0 and M/AC (M = Fe, Co, Ni, Cu, and Zn) surfaces, with values of 0.112, 0.109, 0.091, 0.067 and 0.053 *e*, respectively. Similarly, Bader charge analysis also shows such a result, for example, the electron transfer between Cl_2 and Fe/AC is 0.9489 *e*, much more than that of Hg^0, with 0.610 *e*. So oxidizing gaseous Hg^0 using Cl-containing surfaces is regarded as an effective Hg^0 removal method.

For the oxidation of Hg^0, there are two possible oxidation mechanisms: direct oxidation ($Hg^0 + 2Cl + M \rightarrow HgCl_2 + M$) and two-step oxidation ($Hg^0 + Cl + M \rightarrow HgCl + M$ R1, and $HgCl + Cl + M \rightarrow HgCl_2 + M$ R2). However, the dissociated inclination of HgCl on metal-loaded AC surfaces shows that HgCl is not a stable intermediate, thereby the two-step oxidation mechanism is impossible. Thus, the direct oxidation mechanism of Hg^0 is discussed in the following paragraphs.

The oxidation products (P) are determined on the most favorable adsorption configurations of $HgCl_2$ on metal-loaded AC surfaces. The reactants (R) are the coexistent configurations of Hg^0 and 2Cl-M/AC (M = Fe, Co, Ni, Cu and Zn), in which Hg^0 is in the gas phase except for the R(Co). So only the catalytic oxidation of Hg^0 on 2Cl-M/AC (M = Fe, Ni, Cu and Zn) are considered, with Hg^0 in distances of 5.500, 5.605, 5.499 and 5.499 Å from Fe, Ni, Cu and Zn, respectively. Fig. 11 shows the structures of reactants and transition states (TS), and the product structures are in Fig. 9. The heats of reaction and energy barriers involved in Hg^0 oxidation processes are displayed in Table 5. All configurations have been examined by the TS confirmation and frequency analysis.

Table 5
The energy barriers (E_a, kJ/mol) and heats of reaction (△H, kJ/mol) involved in the oxidation of Hg^0 on 2Cl-M/AC (M = Fe, Ni, Cu and Zn) surfaces.

Catalyst	Hg^0 oxidation pathway	E_a (kJ/mol)	△H (kJ/mol)
Fe/AC	$Hg^0 + 2Cl\text{-}Fe/AC \rightarrow HgCl_2\text{-}Fe/AC(b)$	42.2	11.1
Ni/AC	$Hg^0 + 2Cl\text{-}Ni/AC \rightarrow HgCl_2\text{—}Ni/AC(b)$	108.7	19.0
Cu/AC	$Hg^0 + 2Cl\text{-}Cu/AC \rightarrow HgCl_2\text{—}Cu/AC(b)$	64.1	−1.8
Zn/AC	$Hg^0 + 2Cl\text{-}Zn/AC \rightarrow HgCl_2\text{-}Zn/AC(a)$	102.5	101.9
	$Hg^0 + 2Cl\text{-}Zn/AC \rightarrow HgCl_2\text{-}Zn/AC(b)$	103.0	105.3

Hg^0 in gas approaches to the surface Cl atoms and results in the formation of the oxidation products P[$HgCl_2$-Fe/AC (b)], P[$HgCl_2$-Ni/AC (b)], P[$HgCl_2$-Cu/AC (b)], P[$HgCl_2$-Zn/AC (a)] and P[$HgCl_2$-Zn/AC (b)] according to the Eley-Rideal mechanism, which is different from the Langmuir–Hinshelwood mechanism on the Au(111) surface and V_2O_5-TiO_2 catalyst [56,57]. The energy barriers of 42.2, 108.7, 64.1, 102.5 and 103.0 kJ/mol are needed to overcome at transition states TS(Fe), TS(Ni), TS(Cu), TS(Zn-a) and TS(Zn-b),

respectively. Accordingly, it can be concluded that the Fe-loaded AC is an effective catalyst, which also has a positive impact on adsorptions of H_2S and CO [12,15]. Besides, in the CO_2 methanation at low temperature, the addition of Fe could enhance the catalytic activity of Ni/ZrO_2 more efficiently than that of Co and Cu [58].

4. Conclusion

The density functional theory (DFT) has been adopted to investigate adsorption behaviors of mercury species and Hg^0 catalytic oxidation on Fe/AC, Co/AC, Ni/AC, Cu/AC and Zn/AC surfaces. For the adsorption case, both parallel and perpendicular orientations are considered, indicating that metal-loaded AC surfaces show stronger capturing capacities to Hg^0 than the pure AC surface. The adsorption energy of Hg^0 on the Fe/AC is the largest with 40.3 kJ/mol, but still a physical adsorption. HgCl prefers to dissociate, with Cl binding on metal-loaded AC surfaces strongly and Hg desorbing. The main adsorption modes of $HgCl_2$ on metal-loaded AC surfaces are various. On the Fe/AC surface, $HgCl_2$ inclines to the parallel molecular adsorption, while dissociated adsorption modes are primary on Ni/AC, Cu/AC and Zn/AC surfaces. But both molecular and dissociated adsorptions exist on the Co/AC surface.

The catalytic oxidation of Hg^0 to be molecular or dissociated $HgCl_2$ over the M/AC (Fe, Ni, Cu and Zn) shows an Eley-Rideal mechanism. And Fe/AC is the best catalyst, only needing to overcome an activation energy of 42.2 kJ/mol. So oxidizing Hg^0 by Cl_2 over Fe/AC catalyst is a relatively cost-effective method for Hg^0 capturing.

Acknowledgments

We gratefully acknowledge the assistance of National Natural Science Foundation of China (Grant Nos. 21276171, 21576178 and 21476155), the National Younger Natural Science Foundation of China (Grant No. 21103120) and the Program for the Innovative Talents of Higher Learning Institutions of Shanxi.

References

[1] J. Dong, Z.H. Xu, S.M. Kuznicki, Environ. Sci. Technol. 43 (2009) 3266–3271.
[2] H. Zeng, F. Jin, J. Guo, Fuel 83 (2004) 143–146.
[3] R.N. Sliger, J.C. Kramlich, N.M. Marinov, Fuel Process. Technol. 65 (2000) 423–438.
[4] B. Krishnakumar, J.J. Helble, Environ. Sci. Technol. 41 (2007) 7870–7875.
[5] B.K. Zhang, J. Liu, J.Y. Zhang, C.G. Zheng, M. Chang, Chem. Eng. J. 237 (2014) 344–351.
[6] J. Wilcox, E. Rupp, S.C. Ying, D.H. Lim, A.S. Negreira, Int. J. Coal Geol. 90 (2012) 4–20.
[7] B. Padak, M. Brunetti, A. Lewis, J. Wilcox, Environ. Prog. 25 (2006) 319–326.
[8] D. Ballestero, C. Gómez-Giménez, E. García-Díez, R. Juan, B. Rubio, M.T. Izquierdo, J. Hazard. Mater. 260 (2013) 247–254.
[9] J.W. Wang, J.L. Yang, Z.Y. Liu, Adv. Mater. Res. 347 (2012) 1847–1851.
[10] D.K. Li, J.R. Han, L.N. Han, J.C. Wang, L.P. Chang, J. Environ. Sci. 26 (2014) 1497–1504.
[11] Y.X. Liu, Elemental Mercury Removal from Flue Gas by Metal/Metal Oxide Decorated Graphene Oxide Composites [D], University of Alberta, 2014, 2016.
[12] H.P. Zhang, X.G. Luo, H.T. Song, X.Y. Lin, X. Lu, Y.H. Tang, Appl. Surf. Sci. 317 (2014) 511–516.
[13] A.A. Presto, E.J. Granite, Environ. Sci. Technol. 40 (2006) 5601–5609.
[14] A.S. Negreira, J. Wilcox, J. Phys. Chem. C 117 (2013) 24397–24406.
[15] L. Wang, Q.Q. Luo, W.H. Zhang, J.L. Yang, Int. J. Hydrogen Energy 39 (2014) 20190–20196.
[16] L. Ma, J.M. Zhang, K.W. Xu, V. Ji, Appl. Surf. Sci. 343 (2015) 121–127.
[17] C.M. Ramos-Castillo, J.U. Reveles, R.R. Zope, R.D. Coss, J. Phys. Chem. C 119 (2015) 8402–8409.
[18] Y.H. Zhang, L.F. Han, Y.H. Xiao, D.Z. Jia, Z.H. Guo, F. Li, Comp. Mater. Sci. 69 (2013) 222–228.
[19] S. Nachimuthu, P.J. Lai, J.C. Jiang, Carbon 73 (2014) 132–140.
[20] J.A. Steckel, Phys. Rev. B77 (2008) 115412.
[21] D. Roseborough, M. Göthelid, P. Palmgren, S. Seetharaman, Metall. Mate. Trans. B 37 (2006) 1057–1066.
[22] S.L. Bastow, A Structural Study of Mercury Adsorbed on Single Crystal Metal Surfaces [D], University of Nottingham, 1997, 2016.
[23] S. Aboud, E. Sasmaz, J. Wilcox, Main Group Chem. 7 (2008) 205–215.
[24] B. Wanno, C. Tabtimsai, Super Lattices Microst. 67 (2014) 110–117.
[25] Y.P. Zheng, W. Xiao, M. Cho, K. Cho, Chem. Phys. Lett. 586 (2013) 104–107.
[26] N. Ding, X.Q. Lu, C.M.L. Wu, Comp. Mater. Sci. 51 (2012) 141–145.
[27] M.R. Xia, W. Ding, K. Xiong, L. Li, X.Q. Qi, S.G. Chen, B.S. Hu, Z.D. Wei, J. Phys. Chem. C 117 (2013) 10581–10588.
[28] L. Jeloaica, V. Sidis, Chem. Phys. Lett. 300 (1999) 157–162.
[29] D.H. Lim, J. Wilcox, J. Phys. Chem. C 115 (2011) 22742–22747.
[30] X.Q. Liu, Y. Xue, Z.Y. Tian, J.J. Mo, N.X. Qiu, Appl. Surf. Sci. 285 (2013) 190–197.
[31] P. Cabrera-Sanfelix, J. Phys. Chem. A 113 (2008) 493–498.
[32] L.X. Ling, S.P. Zhao, P.D. Han, B.J. Wang, R.G. Zhang, J. Chem. Eng. 244 (2014) 364–371.
[33] J. Ren, W. Wang, D.L. Wang, Z.J. Zuo, J.Y. Lin, Z. Li, Appl. Catal. A-Gen. 472 (2014) 47–52.
[34] Z.Y. Wang, B. Yang, Y.L. Wang, Y.F. Zhao, X.M. Cao, P. Hu, Phys. Chem. Chem. Phys. 15 (2013) 9498–9502.
[35] A. Hashimoto, K. Suenaga, A. Gloter, K. Urita1, S. Iijima, Nature 430 (2004) 870–873.
[36] S.C. Xu, S. Irle, D.G. Musaev, M.C. Lin, J. Phys. Chem. C 113 (2009) 18772–18777.
[37] Y.Y. Liu, J. Wilcox, Environ. Sci. Technol. 45 (2010) 809–814.
[38] M. Zhou, Y.H. Lu, Y.Q. Cai, C. Zhang, Y.P. Feng, Nanotechnology 22 (2011) 385502.
[39] X. Sun, J.Y. Hwang, S.Q. Xie, Fuel 90 (2011) 1061–1068.
[40] B. Padak, J. Wilcox, Carbon 47 (2009) 2855–2864.
[41] J. Ren, J.Z. Yang, W. Wang, H.L. Guo, Z.J. Zuo, J.Y. Lin, Z. Li, Int. J. Quantum Chem. 115 (2015) 853–858.
[42] L. Yu, X.L. Pan, X.M. Cao, P. Hu, X.H. Bao, J. Catal. 282 (2011) 183–190.
[43] Y.N. Tang, Z.X. Yang, X.D. Dai, J. Chem. Phys. 135 (2011) 224704.
[44] H. Valencia, A. Gil, G. Frapper, J. Phys. Chem. C 114 (2010) 14141–14153.
[45] S.J. Lee, Y.C. Seo, J. Jurng, T.G. Lee, Atmos. Environ. 38 (2004) 4887–4893.
[46] A.V. Krasheninnikov, P.O. Lehtinen, A.S. Foster, P. Pyykkö, R.M. Nieminen, Phys. Rev. Lett. 102 (2009) 126807.
[47] B.K. Zhang, J. Liu, C.G. Zheng, M. Chang, Chem. Eng. J. 256 (2014) 93–100.
[48] P. Guo, X. Guo, C.G. Zheng, Fuel 90 (2011) 1840–1846.
[49] B.G. Kim, X.X. Li, P. Blowers, Langmuir 25 (2009) 2781–2789.
[50] D.H. Lim, S. Aboud, J. Wilcox, Environ. Sci. Technol. 46 (2012) 7260–7266.
[51] Y. Zhao, M.D. Mann, J.H. Pavlish, B.A.F. Mibeck, G.E. Dunham, E.S. Olson, Environ. Sci. Technol. 40 (2006) 1603–1608.
[52] J. Liu, M.F. He, C.G. Zheng, M. Chang, Proc. Combust. Inst. 33 (2011) 2771–2777.
[53] E. Sasmaz, J. Wilcox, J. Phys. Chem. C 112 (2008) 16484–16490.
[54] Y.X. Zhao, M.D. Mann, E.S. Olson, J.H. Pavlish, G.E. Dunham, J. Air Waste Manage. 56 (2006) 628–635.
[55] Y.S. Gao, Z. Zhang, J.W. Wu, L.H. Duan, A. Umar, L.Y. Sun, Z.H. Guo, Q. Wang, Environ. Sci. Technol. 47 (2013) 10813–10823.
[56] D.H. Lim, J. Wilcox, Environ. Sci. Technol. 47 (2013) 8515–8522.
[57] A.S. Negreira, J. Wilcox, J. Phys. Chem. C 117 (2013) 1761–1772.
[58] J. Ren, X. Qin, J.Z. Yang, Z.F. Qin, H.L. Guo, J.Y. Lin, Z. Li, Fuel Process. Technol. 137 (2015) 204–211.